Attosecond imaging of molecules using high harmonic spectroscopy

Peng Peng, Claude Marceau and David M. Villeneuve *

Abstract | The availability of attosecond-duration extreme ultraviolet or soft X-ray light sources has opened up new fields of research in atomic and molecular physics. These pulses can be as short as 50 as, fast enough to freeze the motion of electrons within molecules, to resolve how electrons rearrange themselves after the removal of an electron and to study electron–electron correlations. Gas-phase molecules can be aligned in space using short laser pulses, permitting the measurement of molecular parameters in the molecular frame. Aligned molecules can be photoionized using a train of attosecond pulses, enabling the complete characterization of the partial waves making up the photoelectron angular distributions. Using a recolliding electron in the high harmonic process allows complex transition dipole matrix elements to be recorded (including their amplitude and phase) in the molecular frame. High harmonic spectroscopy makes it possible to image molecular orbitals and for unimolecular chemical reactions to be followed with femtosecond resolution. For example, the behaviour around conical intersections can be probed. Charge migration within molecules can be observed with sub-femtosecond resolution.

The high harmonic generation (HHG) process was first observed in 1987 (REF.[1]): an intense laser was focused into a gas, and odd multiples of the driving laser frequency were detected in the forward direction of propagation of the laser. At first, this was just a curiosity, but as the process became better understood, its utility was recognized. Now HHG can generate isolated attosecond pulses with durations below 50 as (REFS[2,3]). Such isolated attosecond pulses are important in studying the motion of electrons within atoms and molecules and in understanding changes in the optical properties of materials. Unfortunately, isolated attosecond pulses are difficult to generate, requiring a high degree of control of the laser system. However, trains of attosecond pulses are relatively easy to generate with commercial femtosecond laser systems and gas targets in vacuum chambers. A train of attosecond pulses produces a spectrum in the extreme ultraviolet (XUV) region that is composed of odd multiples of the driving laser frequency, whereas isolated attosecond pulses produce a smooth spectrum.

HHG was first thought of as a source of XUV radiation and attosecond pulses. Later, however, it became apparent that the HHG spectrum contained information about the structure of molecules in the gas target. This observation led to the field now called high harmonic spectroscopy.

In this Review, we focus on how high harmonic sources of XUV radiation are used to study the structure and dynamics of atoms and molecules in the gas phase. The reader is directed to review articles on attosecond science for further details[4–10].

Joint Attosecond Science Laboratory, National Research Council and University of Ottawa, Ottawa, ON, Canada.

**e-mail: David.Villeneuve@uottawa.ca*

https://doi.org/10.1038/s42254-018-0015-1

Basics of high harmonic spectroscopy

High harmonics are commonly generated by commercial femtosecond titanium–sapphire laser systems. In the process of HHG, an intense femtosecond laser pulse is focused into a gas target (BOX 1). The laser field ionizes the gas and accelerates the electrons back to the parent ion. If the electron recombines with the ion, it emits a photon whose energy equals the kinetic energy of the electron at recombination plus the binding energy. This process results in the emission of a spectrum consisting of a series of odd multiples of the driving laser frequency. The photon energy of this emission spans the range from 10 eV to 150 eV, called the XUV. HHG can be used as a source of coherent XUV emission, for example, to photoionize atoms or molecules[11–19], or as a source of attosecond-duration pulses to study time delays in photoionization[20–31].

The wavelength of the XUV emission itself is much too long to be used to image the structure of molecules directly. A photon with an energy of 124 eV has a wavelength of 10 nm, whereas a typical molecular bond is only 0.1 nm. Gas-phase electron diffraction requires photon energies of 50 keV, well beyond the range produced by HHG. However, an electron with a kinetic energy of 100 eV has a de Broglie wavelength of 0.12 nm. The recombining electron in HHG has just the right wavelength to be sensitive to the molecular structure. High harmonic spectroscopy is based on HHG, in which the emitted photon provides the output signal from the experiment, but it relies on the recombining electron to 'measure' the molecule (BOX 2).

Key points

- High harmonic spectroscopy uses femtosecond lasers to probe the valence electrons in gas-phase molecules. It records the transition dipole matrix elements upon recombination from a set of continuum wavefunctions. This is effectively time-reversed photoionization in which the highest occupied molecular orbitals are isolated.
- A weaker laser can create rotational revivals that lead to an ensemble of molecules that are aligned in space and are field-free. This allows measuring of the dipole matrix elements in the molecular frame.
- At the sub-optical-cycle level, on the attosecond timescale, electron–electron correlations can be revealed.
- Simple chemical reactions such as unimolecular dissociation and the behaviour around conical intersections can be followed on a femtosecond timescale using pump–probe techniques.
- Charge migration following removal of an electron from a molecule can be visualized with sub-femtosecond time resolution.

An atom can be photoionized by a single photon process if the photon energy exceeds the binding energy of the electron. The probability and angular distribution of the freed electron are determined by the dipole matrix element of the transition from the bound state to the continuum state. Photoelectron spectroscopy is a valuable tool in understanding the electronic states of molecules. At low photon energy, only valence electrons are detached. As the photon energy increases, more deeply bound electrons are liberated, until finally the K-shell electrons of the constituent atoms are removed. By contrast, when an intense infrared laser is used to ionize a molecule in a multiphoton process, only valence electrons can be removed, because the ionization probability scales exponentially with the binding energy. This means that the first step in HHG selectively chooses the valence electrons. Valence electrons are responsible for molecular bonds and the chemical behaviour of molecules.

The third and final step of HHG is the recombination of the electron with the parent ion. If the atom or molecule ends up in the same quantum state as it began, then the emission has a definite phase relationship with the driving laser field, and the emission will be coherent with the driving field. This is a necessary but not sufficient condition for the emission to be phase-matched, which is a collective property of the build-up of the XUV field through the medium. Recombination can also occur to excited states, but such emission will not be phase-matched and will be much weaker than the phase-matched emission. In this way, HHG selects only valence electrons and ensures that they recombine to their initial state.

The process of HHG can be approximately factorized in the frequency domain[32–35]:

$$S(E_\Omega) = I(F,\omega)W(E)\sigma(E) \quad (1)$$

Here, S is the power spectrum emitted from a single molecule, I is the ionization probability for a given driving laser field F and frequency ω, W describes the propagation of the free electron with kinetic energy E upon return and σ is the recombination cross section. A range of electron kinetic energies (E) are produced, and so the cross section is simultaneously measured for a wide range of E. E_Ω is the photon energy corresponding to the recolliding electron kinetic energy E. The first two terms are only weakly dependent on the target molecule, whereas the recombination cross section depends critically upon the details of the molecule and the electronic state involved. It is this cross section that gives high harmonic spectroscopy its utility.

High harmonic spectroscopy in atoms

Because the HHG process involves the photorecombination of the electron, the transition dipole moment between a bound electronic state and a set of continuum states is invoked (the cross section σ is proportional to the square of the transition dipole moment). Photorecombination can be considered as a time-reversed version of photoionization in which the electron is selected by tunnel ionization by the laser field.

A simple demonstration of high harmonic spectroscopy is the observation of a Cooper minimum. In photoionization, a Cooper minimum[48] occurs at a particular photon energy in which the ionization probability has a minimum[49]. The argon atom has a prominent Cooper minimum at around 50 eV. When argon is used as the target in HHG experiments, a minimum is clearly seen in the emitted spectrum around the Cooper minimum[50–56]. This result demonstrates that photoionization and photorecombination share the same transition dipole moment.

Less intuitively, HHG reproduces the giant resonance in xenon around 100 eV that is seen in synchrotron experiments[57,58] (FIG. 1a). The giant resonance involves electron–electron correlations between the detached electron and deeply bound electrons[34,35,59,60]. The photoionization cross section at 100 eV is weak from the valence 5p shell but strong from the deeper 4d shell. In photoionization, a 4d electron interacts with a 5p electron as it departs, leading to the 5p electron filling the 4d hole. The process is similar in HHG but reversed in time. The driving laser field is not able to remove a deeply bound 4d electron and can remove only a 5p electron. In recombination, the electron can excite a 4d electron to fill the 5p hole, and the electron recombines into the 4d hole with its greater cross section.

High harmonic spectroscopy in aligned molecules

Unlike atoms, molecules have a geometric structure that affects the electronic transitions. For example, electronic transitions in a linear molecule will be different for an electric field that is polarized parallel or perpendicular to the molecular axis. It is possible to align gas-phase molecules in space using femtosecond laser pulses[63,64]. A laser field whose intensity is less than that required to ionize the molecule will, through a series of rotational Raman transitions, create a superposition of rotational states. After the laser pulse, the rotational states will evolve in time and, at particular times, will rephase to create an aligned ensemble of molecules. The periodic rephasings are called molecular revivals. For example, in nitrogen molecules, the molecular axes will line up with the polarization direction 8.2 ps after the aligning laser pulse. By rotating the polarization direction of the aligning laser, it is possible to align the molecular axis in a chosen direction, permitting measurements in the molecular reference frame.

Box 1 | **High harmonic generation**

The first attosecond-duration electromagnetic pulses were created by high harmonic generation (HHG)[36,37]. In HHG, an intense femtosecond laser is focused into a gas, for example, helium. If the focused intensity exceeds 5×10^{14} W cm^{-2}, then the electric field of the laser exceeds the binding energy of the electron, resulting in the ionization of the atom. In the few femtoseconds following ionization, the detached electron moves under the influence of the laser field, first moving away from the ion, then moving back towards it. The returning electron can elastically scatter, inelastically scatter or recombine to form a neutral atom. The third option is very unlikely (probability of ~10^{-6}) but results in the emission of a photon. The photon energy is the sum of the electron kinetic energy just before recombination and the binding energy of the final state. For typical titanium–sapphire femtosecond lasers, this can produce photons with energies from 10 eV to 150 eV. Longer-wavelength lasers accelerate the electrons to greater kinetic energy, making keV photons possible[38]. The three-step process[39] of HHG that takes place during a single optical cycle is illustrated below (see the figure, panel **a**).

The process of ionization and recombination takes place for many atoms in the laser focus. Remarkably, the emitted photons are produced simultaneously with the driving laser's electric field, and so the emitted electromagnetic field from all the atoms is coherent. In order to extract quantitative information about the recombination dipole moment, it is necessary to ensure that phase mismatch between the driving field and the extreme ultraviolet (XUV) field does not occur. This can be achieved by using a medium whose length is shorter than the phase-matching length[40], ensuring that the XUV emission builds up coherently in the medium. This leads to phase-matched emission from the entire gas sample that is collimated in the forward direction (see the figure, panel **b**). See also the Supplementary Video.

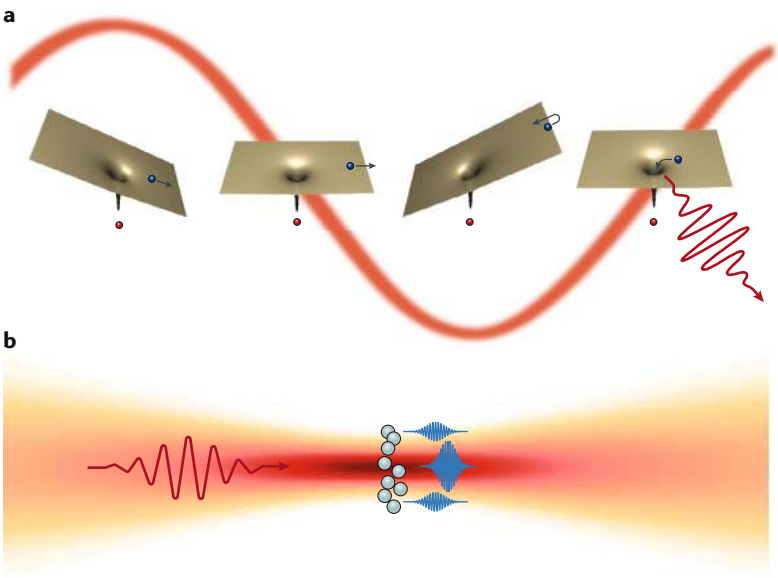

As was the case with atoms, the high harmonic spectrum contains the signature of the target molecule[65–68]. The angular variation in the spectrum is different for the three molecules shown in FIG. 1b. For example, the emission from N_2 maximizes when the molecular axis is parallel to the polarization axis of the driving laser, whereas for CO_2, the emission maximizes for the perpendicular orientation[61]. It is possible to orient polar molecules using a combination of laser fields[69], and high harmonic spectroscopy in the oriented molecular frame is then possible[70–74]. For oriented molecules, the asymmetry of the molecule leads to the emission of even harmonics in addition to the usual odd harmonics. The even harmonics are a measure of the phase difference in the emission from each end of the molecule.

Certain linear molecules can be considered two-centred, that is, the highest occupied molecular orbital (HOMO) can be written as the sum of the same wavefunction ψ_a:

$$\psi(r) = \psi_a\left(r - \frac{R}{2}\right) \pm \psi_a\left(r + \frac{R}{2}\right) \quad (2)$$

Here, R is the separation between the two centres. For the plus sign, the molecule is symmetric, whereas for the minus sign, the molecule is antisymmetric. The CO_2 molecule is an example of the antisymmetric case owing to the π_g-symmetry of the HOMO. Such molecules are expected to have different high harmonic spectra because interferences can occur in the recombination step[62,75–77], as illustrated in FIG. 1c for the case of CO_2. The recolliding electron has a de Broglie wavelength that depends on its kinetic energy and thus on the emitted photon energy. If the electron wave returns to the molecule at an angle θ to the molecular axis, there will be destructive interference upon recombination at both oxygen atoms when $R\cos\theta = \lambda$, where R is the separation between the oxygen atoms and λ is the energy-dependent de Broglie wavelength of the electron. For CO_2 at 30°, the minimum should occur around 65 eV.

The polar plot for CO_2 in FIG. 1b shows a clear interference pattern. At 0°, at which the molecular axis is parallel to the polarization axis, a minimum in emission is evident at around 30 eV. At first, this was thought to be a structural minimum, that is, a minimum caused by the quantum interference between the two atoms[62,75]. It was later noted that the position of this minimum was dependent on the laser intensity, suggesting that it was not a result of a structural feature but instead is a dynamic minimum[78–81]. The actual structural minimum becomes evident around 65 eV using a longer laser wavelength. Another example of multiple orbital contributions to HHG is in N_2, from which the signal from HOMO-1 became apparent[82–84].

In addition to recording the intensity of each harmonic order, it is also possible to record the phase using a technique called RABITT (reconstruction of attosecond beating by interference of two-photon transitions)[85,86]. In molecular RABITT[24–28], a second gas target is photoionized with the harmonic orders from the first gas jet, and the photoelectrons are dressed by the same infrared laser field that created the harmonics. The modulation of the sidebands versus time delay gives a measure of the phase difference between harmonic orders. It is also possible to make interferometric measurements[87,88] to determine the phase. There are two components to the phase of a harmonic order: the phase as a function of molecular angle and the phase as a function of photon energy (harmonic phase), that is, $\varphi(\theta, q)$. The angular dependence of the harmonic phase can be determined by two-source interferometry[87], in which two nearby HHG sources in the gas jet interfere and, in one of the sources, the molecules are aligned. The dependence of the phase on harmonic order is more difficult to measure; a RABITT approach is generally needed. However, a homodyne signal from a mixture of gases can also be

Box 2 | **Continuum wavefunction**

When an atom is subject to an intense laser pulse, it can be ionized. Quantum mechanically, it can be both ionized and not ionized at the same time. The wavefunction that describes the electron is initially bound to the nucleus. For example, the electron in a hydrogen atom will be in a 1s orbital. The intense electric field of the laser will cause the electronic population to tunnel through the Coulomb barrier. The figure shows frames from a movie based on a time-dependent Schrödinger calculation of a hydrogen atom in a horizontally polarized laser field. The intensity of the image is proportional to the logarithm of the square of the wavefunction, while the colour shows the phase. In panel **a** of the figure, the electronic population tunnels from the atom into the continuum. In panel **b** of the figure, a circular 'watershed' appears; the electronic population to the right never returns to the nucleus, whereas the population to the left is being pushed back to the nucleus, as the laser electric field has reversed direction. In panel **c** of the figure, the atom begins to ionize towards the left in the next optical half-cycle. At the same time, the continuum wavefunction moves from right to left and washes over the nucleus. In panel **d** of the figure, the kinetic energy of the recolliding electron from the right increases. The kinetic energy first increases to a maximum determined by the laser intensity and wavelength and then decreases again. With proper phase matching of the high harmonic generation process, only the increasing (positively chirped) part of the recolliding wavefunction is seen experimentally. This provides a mapping of emitted photon energy to recollision time on a sub-femtosecond scale. As the continuum electron washes over the bound part of the wavefunction, it adds and subtracts coherently, leading to an oscillation in the electron's position in the vicinity of the nucleus. This oscillating charge leads to emission of an electromagnetic wave that chirps up in frequency. These attosecond bursts are produced during each half-cycle of the optical field.

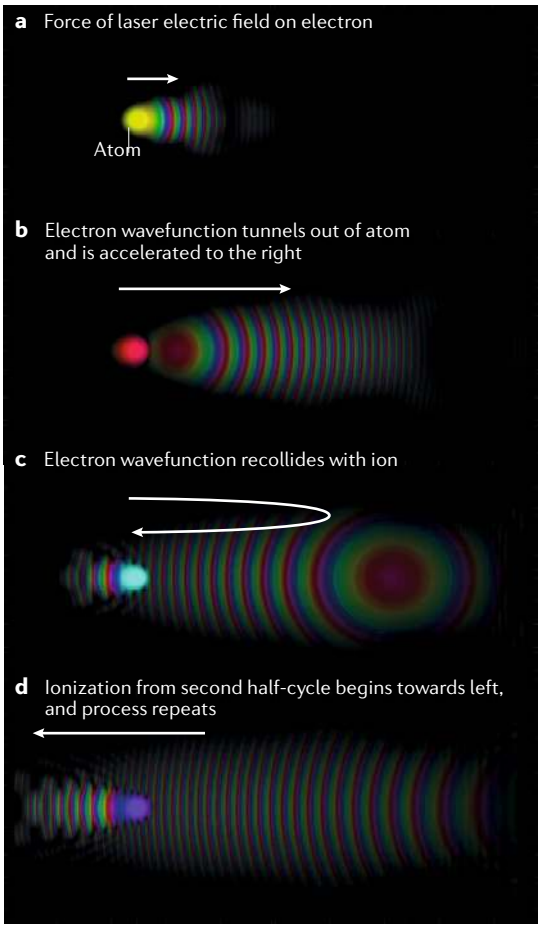

used to resolve the harmonic phase[89,90]. Both of these techniques were combined[88] to completely determine $\varphi(\theta, q)$ in bromine molecules.

Orthogonal two-colour fields can also be used to determine molecular structure and symmetry[91–95]. A strong field at 800 nm is perturbed by a weaker 400 nm pulse that is polarized orthogonally. The second harmonic field perturbs the electron trajectories, breaks the symmetries and leads to the emission of even harmonics. This approach was used to observe the HOMO and HOMO-1 of CO_2 molecules[96].

The polarization state of the emitted harmonics contains additional information[97,98]. If the recolliding electron is at an angle to the molecular axis, and if there is a relative phase between the parallel and perpendicular components of the recombination dipole moment, then the emission will be elliptically polarized.

High harmonics from counter-propagating, circularly polarized two-colour laser fields have circular polarization[99–101]. Spin angular momentum, energy and momentum conservation selection rules determine the handedness of individual harmonic orders and which harmonic orders are emitted. Orbital angular momentum (OAM) is also conserved in HHG. A fundamental beam with one unit of OAM will generate harmonics with OAM equal to their harmonic order[102,103]. Any unexpected deviation from the spin angular momentum and OAM selection rules indicates correlation (exchange of angular momentum) between the light beam and the emitting medium and is influenced by its symmetry.

To summarize, high harmonic spectroscopy contains information across the HHG spectrum on the amplitude, phase and polarization in the molecular frame. This information can be used to reconstruct an image of a molecular orbital.

Tomographic reconstruction of molecular orbitals

If the high harmonic spectrum emitted from an aligned molecule is distinctive and contains information about the transition dipole matrix elements, then it should be possible to determine the bound state wavefunction. This process is similar to tomographic imaging, in which an image is reconstructed from a series of angular projections through the object. Hence, it is dubbed molecular orbital tomography[32].

The reconstruction is based on the factorization of the high harmonic spectrum (see equation 1). The recombination cross section σ is proportional to the square of the transition dipole moment between the single-electron wavefunction ψ_m of the orbital that was ionized by the driving laser and the continuum wavefunction ψ_e:

$$d = <\psi_m|r|\psi_e> \quad (3)$$

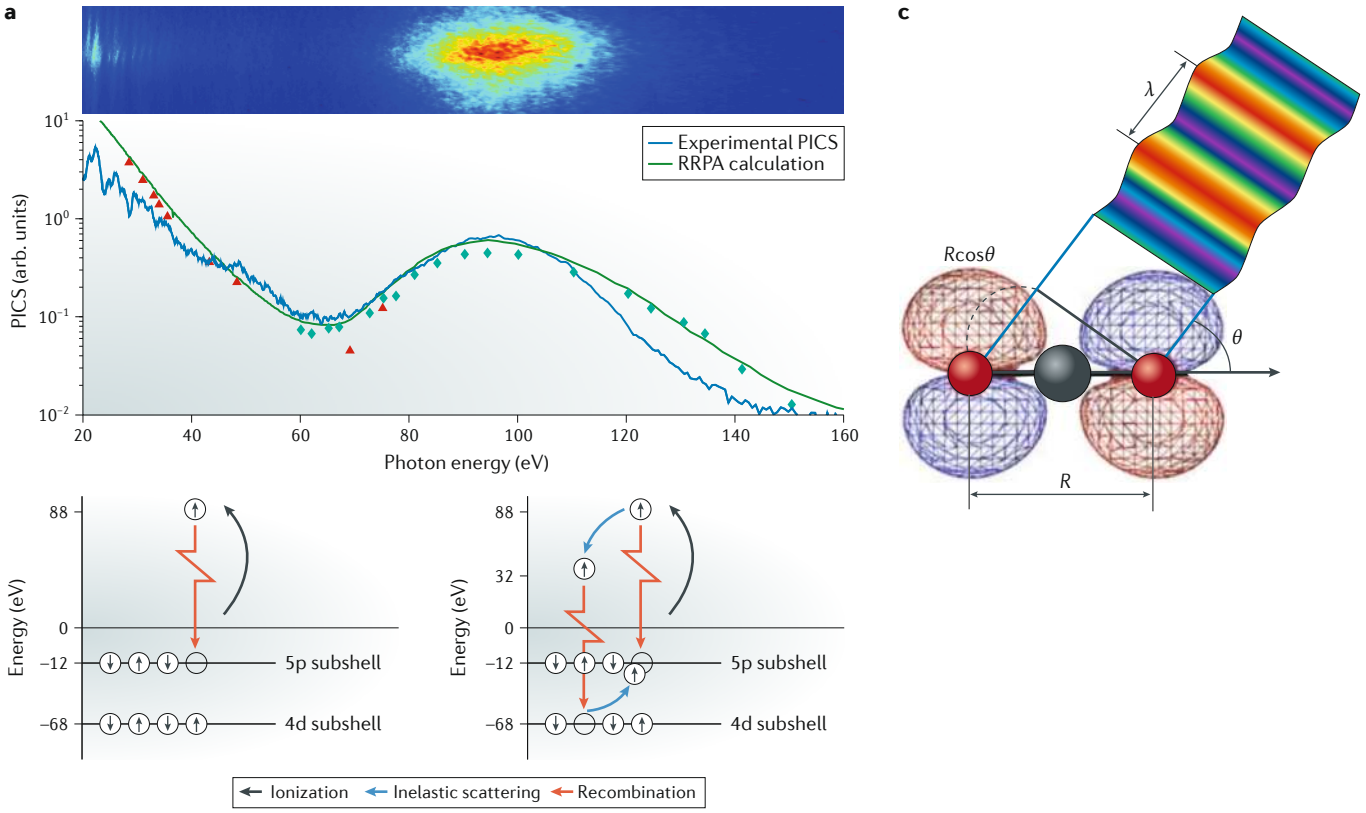

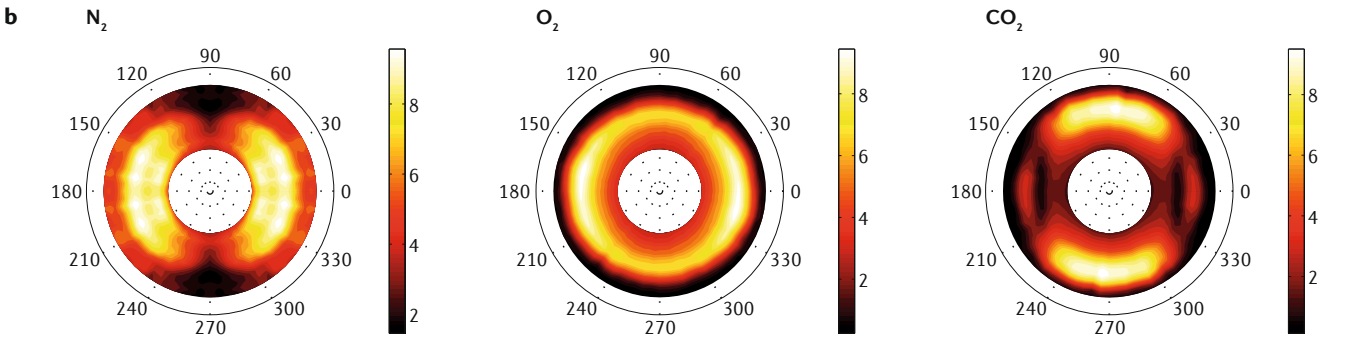

Fig. 1 | **High harmonic spectra from atoms and molecules reveal details of the electronic structure of valence orbitals.** **a** | High harmonic spectrum from xenon gas irradiated with a 1,800 nm laser pulse. The high harmonic generation (HHG) spectrum is the dark blue line and closely follows the cross sections measured in synchrotron experiments (symbols) and a relativistic random phase approximation (RRPA) calculation (green line). The lower portion shows the mechanism by which the 4d electrons are involved in the HHG process, even though the laser removes only a 5p electron. The bottom-left panel shows the usual model of HHG, where a 5p electron is removed by the laser field and then recombines. The bottom-right panel shows how the recolliding 5p electron interacts with a 4d electron through a Coulomb interaction, causing the 4d electron to be excited and fill the 5p hole. The free electron then recombines with the 4d hole, benefitting from the higher transition moment. **b** | High harmonic spectra of molecules N_2, O_2 and CO_2 in the molecular frame. The gas-phase molecules were aligned impulsively with a 100 fs, 800 nm laser pulse. At a delayed time, when the rotational wavepackets rephased, an ensemble of aligned molecules resulted. The laboratory frame alignment angle was controlled by the polarization direction of the aligning pulse. A second, more intense, 800 nm laser pulse ionized the molecules and generated an HHG spectrum. The spectrum is plotted in polar coordinates. The horizontal axis denotes where the HHG pulse's polarization axis is parallel to the molecular axis; the radius covers harmonic orders 0–50. All three molecules exhibit a unique structure in the HHG pattern, an indication that high harmonic spectroscopy is sensitive to the electronic structure of molecules. **c** | Illustration of two-centre interference in the recombination step of HHG. The returning electron is illustrated by the coloured wave with de Broglie wavelength λ approaching the CO_2 molecule. The highest occupied molecular orbital of CO_2 has π_g-symmetry, with orbitals centred on the oxygen atoms. If the separation of the oxygen atoms is R and the electron returns at angle θ relative to the molecular axis, then the returning electron wavefunction will be in phase at the two atoms if $n\lambda = R\cos\theta$. Because of the π_g-symmetry of the orbital, the emitted recombination radiation will be out of phase from the two centres, leading to a minimum in the HHG signal for that particular de Broglie wavelength. This causes a minimum in the HHG spectrum at that angle. PICS, photoionization cross section. Panel **a** is adapted from REF.[59], Springer Nature Limited. Panel **b** is adapted with permission from REF.[61]., Taylor & Francis Ltd. Panel **c** is adapted from REF.[62], Springer Nature Limited.

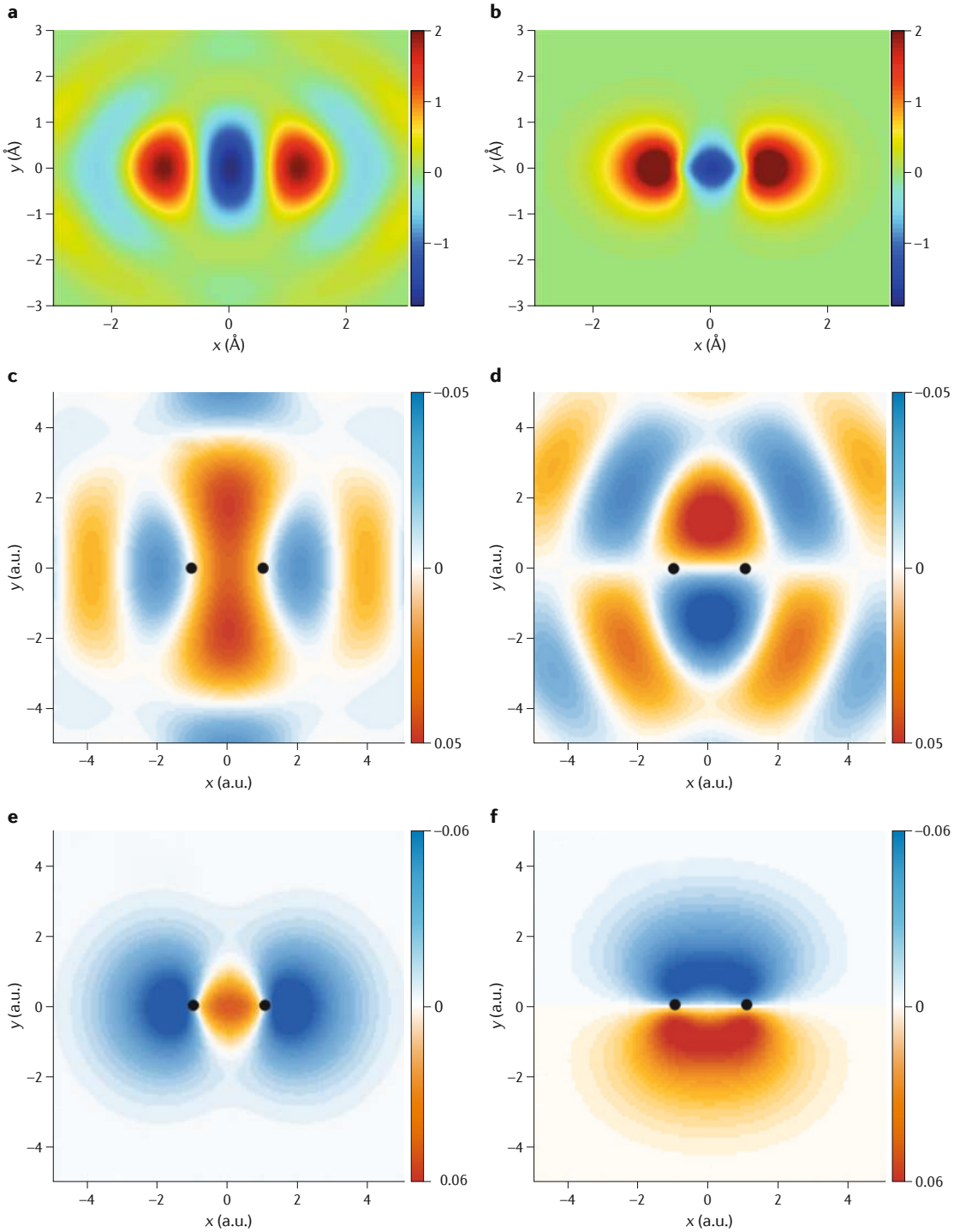

Fig. 2 | **Tomographic imaging of molecular orbitals reveal the structure of a single orbital wavefunction.** **a**,**b** | Image of the highest occupied molecular orbital of a N_2 molecule. The molecular axis is horizontal. Panel **a** shows the orbital image as derived from the experimental high harmonic spectra at a range of angles using the tomographic reconstruction algorithm. Panel **b** shows the $3\sigma_g$ orbital as calculated with a quantum chemistry package. This is an image of the wavefunction, not the electron density; both positive and negative lobes are seen. **c–f** | Reconstructed images of the highest two molecular orbitals of N_2. Both the amplitude and phase of the harmonic orders were recorded, allowing the phase of the recombination dipole moment to be determined. The highest orbital was recovered by using the imaginary part of the recombination dipole and imposing σ_g-symmetry (panel **c**). The second highest orbital used the real part of the recombination dipole and assumes π_u-symmetry (panel **d**). The corresponding orbitals were calculated with a quantum chemistry package (Panels **e**,**f**). Panels **a** and **b** are adapted from REF.[32], Springer Nature Limited. Panels **c–f** are adapted from REF.[105], Springer Nature Limited.

In the single-electron approximation used here, ψ_m can be thought of as a Hartree–Fock orbital. More accurately, it is the Dyson orbital of the remaining ion after the electron has been removed and after the other electrons have relaxed. The continuum wavefunction ψ_e represents the same electron but in the continuum. Quantum mechanically, the electron both remains in the molecule and is removed from the molecule at the same time. The total wavefunction is the sum of the bound and continuum parts. At ionization time, the continuum wavefunction is close to the ion, but as the electron is accelerated by the laser electric field, it spreads laterally, such that it resembles a plane wave when it returns.

For an emitted photon of energy $\hbar\Omega$, the momentum of the corresponding electron is $\hbar k_\Omega = \sqrt{2m_e(\hbar\Omega - E_i)}$. Here, E_i is the binding energy of the electron and m_e is the mass of the electron. This equation establishes the mapping between the photon energy that is recorded in the high harmonic spectrum and the momentum of the electron just before it recombines. The continuum electron wavefunction is approximated by a plane wave, $\psi_e = e^{-ikx}$. Here, x is the polarization direction of the driving laser. Expanding equation 3 as an integral (and, for simplicity, dropping the out-of-plane coordinate z), and noting that the complex exponential in ψ_e gives a Fourier transform:

$$d_\Omega(\theta) = \int_{-\infty}^{\infty}\int \psi_m(r,\theta) r e^{-ik_\Omega x} dx dy = FT\left\{\int_{-\infty}^{\infty} \psi_m(r,\theta) r dy\right\} \quad (4)$$

This expression squared is included in the high harmonic spectrum at frequency Ω at molecular angle θ. By recording a spectrum of Ω at a range of angles θ, it is possible to invert this equation and to determine $r\psi_m$ and hence ψ_m (REF.[32]).

Before doing so, we need to account for the prefactors in equation 1. The prefactors are related to the ionization process and to the propagation of the electron in the laser field. We make the assumption that these two factors are largely independent of the target molecule. We record a high harmonic spectrum of a reference atom, $S_\Omega(\mathrm{Ar})$, to determine these factors. Argon was chosen in the initial experiment, because its ionization potential matched that of the target molecule N_2. Because we know the 3p orbital of argon, we can calculate the transition dipole $d_\Omega(\mathrm{Ar})$. Then, the dipole moment of N_2 is the ratio of the recorded high harmonic spectrum at each angle θ, $S_\Omega(\theta)$, times the dipole moment of argon:

$$d_\Omega(\theta) = d_\Omega(\mathrm{Ar})\sqrt{\frac{S_\Omega(\theta)}{S_\Omega(\mathrm{Ar})}} \quad (5)$$

The dipole moment is a complex quantity; the experimental amplitude does not contain the phase; this is discussed in the following paragraph. This procedure has the advantage that it accounts for the prefactors related

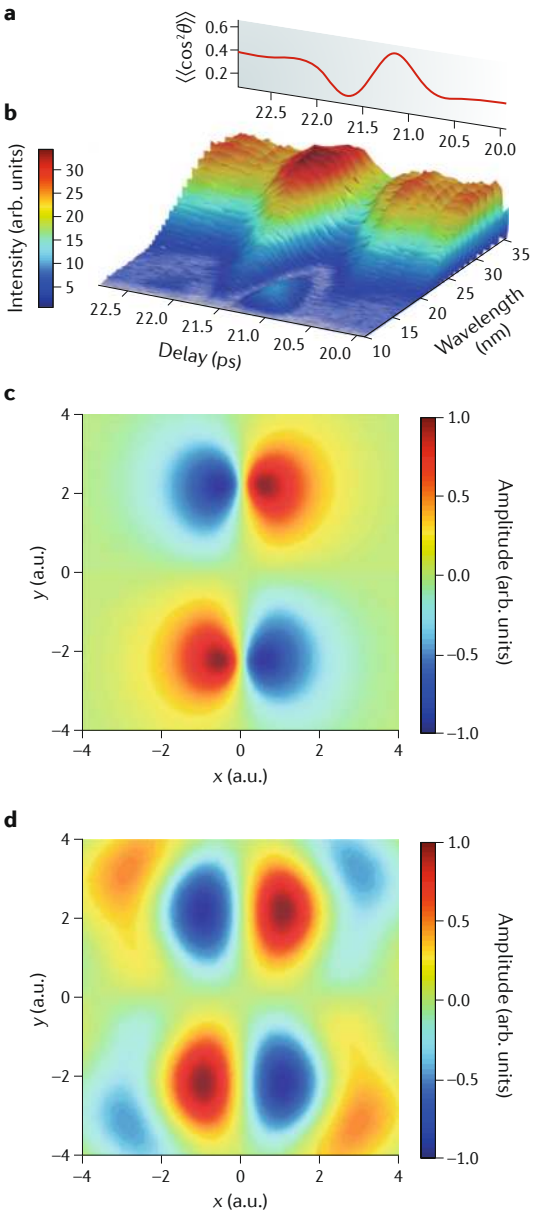

Fig. 3 | **High harmonic spectra from aligned CO_2 molecules driven by an infrared laser. a** | A laser pulse is used to create a rotational revival around 21 ps, when a second pulse with a wavelength of 1,450 nm is used to generate a high harmonic spectrum. **b** | The longer wavelength, compared with 800 nm laser sources, generates a spectrum up to 120 eV. At 21.2 ps, the molecules are aligned parallel to the infrared laser polarization axis, while at 21.6 ps, they are perpendicular. Around the parallel alignment time, a valley appears that is associated with two-centre interference based on the molecular geometry, rather than dynamical interference between orbitals. **c**,**d** | Reconstructed highest occupied molecular orbital of CO_2 deduced from the high harmonic measurements in panel **b**. Using a generalized tomographic reconstruction procedure, the reconstructed orbital in panel **d** is quite similar to the calculated one in panel **c**. The molecular axis is vertical. Adapted from REF.[107], Springer Nature Limited.

to the electron propagation and accounts for experimental details such as detector spectral response.

We now have the Fourier transform along x of a projection along y of the unknown $r\psi_m$. The Fourier slice theorem says that the Fourier transform of a projection equals a cut at angle θ through the 2D transform of the object. This is the essence of computed tomography based on the inverse Radon transform. By applying this transform to the data (an array of values versus Ω and θ), we can deduce $r\psi_m$ and hence ψ_m. The measurement as presented here does not include the phase of the dipole moments. The assumption was made that the dipole was imaginary and had a sign change at 40 eV, at which the amplitude is at a minimum. The resulting reconstructed molecular orbital is shown in FIG. 2a,b. Phase retrieval algorithms can be applied to amplitude-only measurements without a direct phase measurement to extract the orbital shape[104].

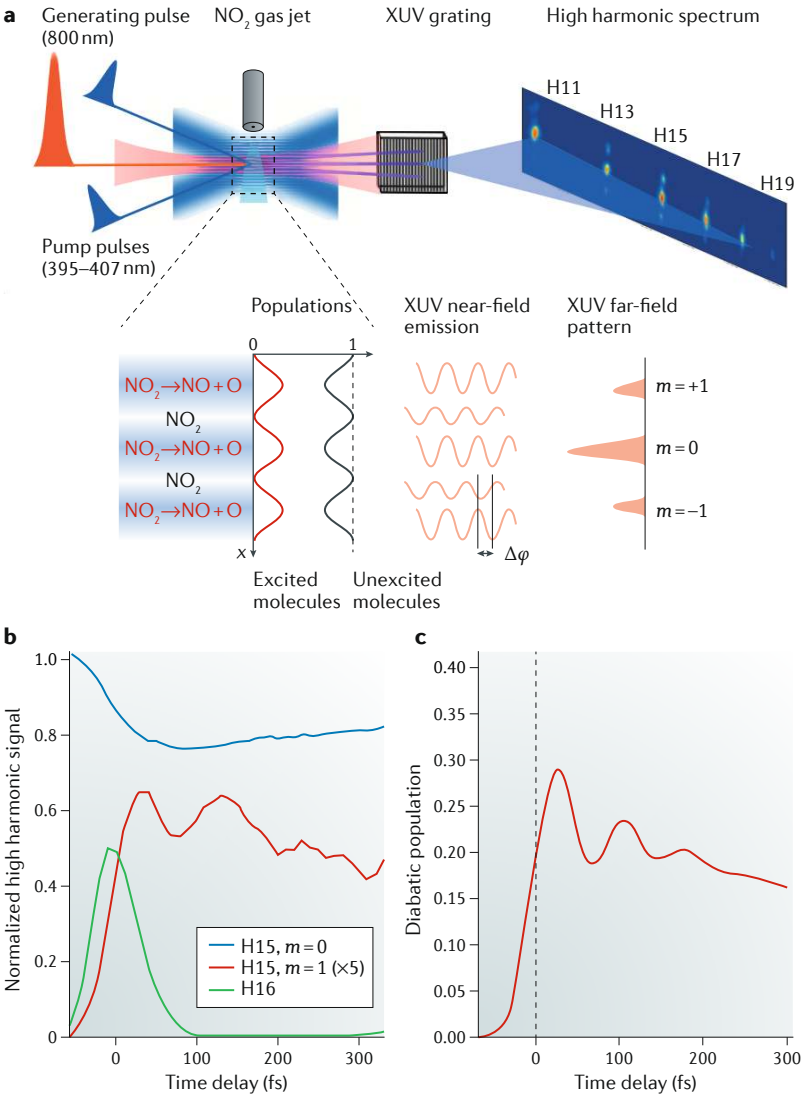

Fig. 4 | **High harmonic spectroscopy using a transient excitation grating reveals nuclear dynamics. a** | Experimental arrangement used to produce a transient grating of excited molecules in a gas jet. The 400 nm pump pulses impinge on the gas jet from above and below, creating an interference pattern in the focus. The interference creates zones of alternating excited and unexcited molecules. The 400 nm pump caused the NO_2 molecules to dissociate. A delayed, intense, 800 nm pulse produced a high harmonic spectrum that was dispersed in a spectrometer. Owing to the periodicity of the population grating, off-axis emission was phase-matched. The off-axis emission contained information about the difference in phase (ϕ) and amplitude between the emissions of the dissociating and unexcited molecules. **b**,**c** | Excited state populations observed with high harmonic spectroscopy in NO_2 molecules. Using a transient grating excitation scheme, a 400 nm pump pulse excited NO_2 molecules, which then began a complicated motion consisting initially of a bending mode. The vibrational wavepacket then travelled through the vicinity of a conical intersection between electronic states, where the electronic population could be exchanged. The off-axis high harmonic emission was a measure of the electronic population on the upper diabatic electronic state. Modulation in time of this signal mirrored the population transfer each time that the conical intersection was encountered. Panel **b** shows the experimental measurement, while panel **c** shows the theoretical modelling (the dotted line marks time zero). $m = 0$ and $m = \pm 1$ represent the undiffracted and diffracted components of each high harmonic order, respectively. Adapted with permission from REF.[111], AAAS.

In another experiment, CO_2 molecules were aligned, and HHG was driven by a laser with a wavelength of 1,450 nm (REF.[107]; see FIG. 3). This laser granted a higher electron kinetic energy and provided HHG spectra to 120 eV. This removed the contributions from lower orbitals because the laser intensity was lower, making the ionization of deeper orbitals less likely, and because the multiple orbit interference occurs near the cut-off frequency. In this case, the two-centre interference is clearly seen around 60 eV, and its position is independent of the laser intensity and wavelength. FIGURE 3b shows the harmonic spectrum versus the time delay from the aligning pulse. As the molecules go through alignment around 21 ps, the structural minimum becomes apparent. Using a phase retrieval algorithm to determine the angular dependence of the phase, making assumptions about the spectral phase and applying a generalized molecular orbital tomographic procedure, the HOMO orbital of CO_2 was retrieved (FIG. 3d).

Following chemical reactions

Given that high harmonic spectroscopy is sensitive to the electronic structure of a molecule, it should be possible to observe changes in a molecule as it undergoes a unimolecular chemical reaction[108]. The HHG inherently has sub-femtosecond time resolution because the recolliding electron is chirped in energy during the optical cycle, mapping emission frequency to time. An example of this is the observation of changes in bond length initiated by the removal of the electron by the driving laser[109,110]. Here, the stretching of the hydrogen bond in H_2 and CH_4 was seen in a time window of 0.9 fs to 1.4 fs by comparing with deuterated isotopes.

Because HHG is driven by femtosecond-duration laser pulses, it is inherently suited to pump–probe experiments. A pump pulse, usually ultraviolet, initiates a unimolecular reaction in a gas-phase molecule. At various delay times, a probe pulse interrogates the molecule by generating an HHG spectrum. The changes in the spectrum are related to the changes that occur in the molecule caused by the pump pulse.

Box 3 | **Generating individual attosecond pulses**

In BOX 1, the high harmonic generation (HHG) process is described as a process in which the photons are emitted by the recombination of electrons with ions. The ionization takes place near the peak of each oscillation of the laser's electric field and thus the process of recombination also takes place during every optical half-cycle of the driving laser. This means that a train of attosecond pulses is created. Because this train of pulses has a periodicity of half of the optical cycle period in the time domain, in the frequency domain, it will have a periodicity of twice the optical frequency. Owing to the alternating parity of each attosecond pulse (left–right alternation of recollision), the spectrum will show peaks at odd integer multiples of the driving laser frequency. For a titanium–sapphire laser with a wavelength of 800 nm and a photon energy of 1.55 eV, the emitted spectrum will be odd multiples of 1.55 eV. This is where the name high harmonic generation came from.

The number of attosecond pulses in the pulse train depends on the duration of the driving laser pulse. By using a very short laser pulse, single, isolated attosecond pulses are created. Pulse durations as short as 50 as have been observed[2–6,41–47].

The HHG emission shows a train of ~5 as-duration pulses (blue) produced by the driving laser field (red) (see the figure, panel **a**). The resulting HHG power spectrum covers the range of 20–80 eV (see the figure, panel **b**). The time–frequency plot (see the figure, panel **c**) shows that the individual attosecond pulses chirp upwards in frequency; this is called the attochirp. XUV, extreme ultraviolet.

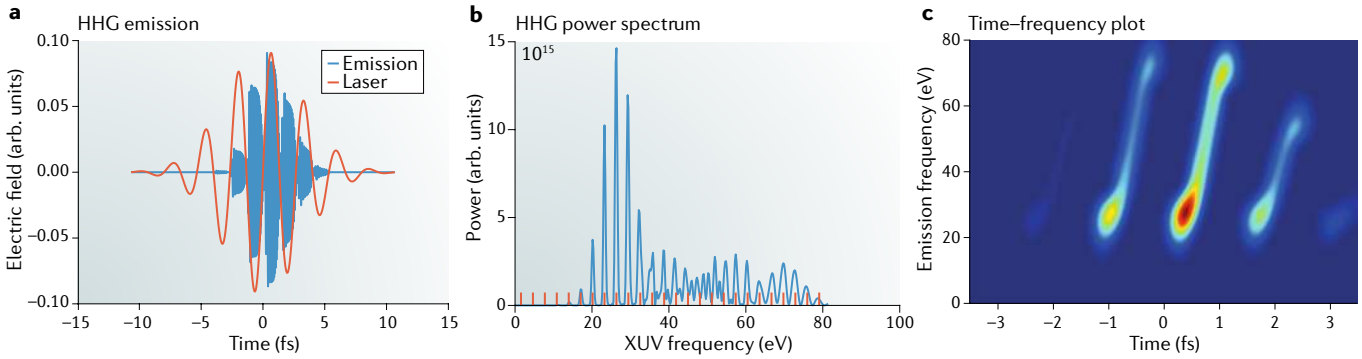

A further advantage of high harmonic spectroscopy is its coherence properties. If the pump pulse is split in two and is focused into the target gas jet at oblique angles, a transient grating is produced in the gas jet, as shown in FIG. 4a. Owing to the interference fringes caused by the two beams, there are alternating regions in which the molecules are excited and not excited by the pump beam, called a population grating. When the probe pulse interrogates the medium, any difference in the generated high harmonic emission, either in amplitude or phase, will produce off-axis emission in addition to the usual on-axis emission. If the spectrometer that detects the XUV light has imaging capabilities along the slit direction, then the on-axis and off-axis emission can be seen separately. The transient grating is particularly sensitive to phase differences, making it possible to record both the amplitude and phase differences of the excited molecules compared with those of the unexcited ones.

Transient grating high harmonic spectroscopy was applied to study the dynamics around a conical intersection in the NO_2 molecule[111]. Upon absorbing a 400 nm photon, the NO_2 molecule is excited electronically, leading to a decrease in the bend angle. The vibrational wavepacket then crosses through a conical intersection with the ground electronic state, at which point the electronic population can either remain on the excited state or transfer to the ground state. The vibrational wavepacket can return to the vicinity of the conical intersection several times. The off-axis high harmonic signal was found to modulate with a period of ~120 fs, which was associated with the electronic population on the diabatic excited state (FIG. 4b,c). It was concluded that high harmonic spectroscopy in a diatomic molecule[112] is associated with the vibrational wavepacket dynamics, whereas in polyatomic molecules[111,113], it is sensitive to the electronic state of the molecule. This is because the wavepacket motion in a diatomic molecule is restricted to one dimension, and thus variation in the ionization probability or Franck–Condon factors will modulate the HHG signal. In polyatomic molecules, the wavepacket quickly disperses in three dimensions, reducing the dependence on the wavepacket location.

Electronic charge transfer in molecules

As described in the previous section, a pump pulse can initiate geometric changes in a molecule. High harmonic spectroscopy can also observe purely electronic features. A superposition of electronic states creates an electronic wavepacket that oscillates with a frequency given by the energy separation of the electronic states. An experiment demonstrated this in NO molecules[114], in which an excited electronic state was weakly populated by stimulated Raman scattering. The high harmonic emission modulated at the expected frequency of the electronic wavepacket. HHG depends on the coherence of the emission to provide phase matching in the forward direction. In general, different initial electronic states can lead to HHG, but the emission is as if different molecules are emitting independently from each initial state. This was the case for the dynamic interference between orbitals in CO_2 (REF.[79]). However, if the initial electronic states are populated coherently, then cross terms are possible in the HHG spectrum. That was the case in the NO experiment[114]. The cross terms involve ionization from one initial state and recombination to the other initial state. High harmonic spectroscopy is a powerful tool because it is sensitive to electronic coherences in the molecule.

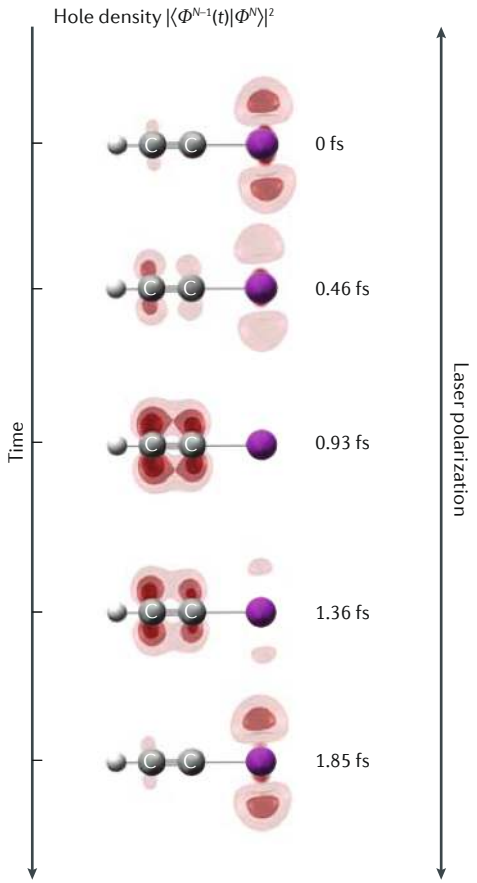

Fig. 5 | **Reconstructed electron dynamics following ionization of iodoacetylene.** The molecule is first oriented in space, that is, its molecular axis is aligned, and the iodine end is preferentially pointing in one direction. The inversion symmetry of the high harmonic generation process is now broken, leading to the emission of both even and odd harmonic orders. The ratio of even to odd order intensities contains information about their phase difference. Using the time-to-frequency mapping from the attochirp, the motion of the electron hole can be determined. The strong laser field removes the electron from the iodine end of the molecule. The hole then travels the length of the molecule and returns to the iodine end in 1.85 fs. Φ^N and $\Phi^{N-1}(t)$ are the N and $N-1$ electron wavefunctions of the neutral and ionized molecule, respectively. Adapted with permission from REF.[120], AAAS.

Electronic wavepackets that are of most interest are usually much faster than those created in NO. For example, charge transfer and charge migration in molecules are important in the understanding of chemical processes yet occur on a longer femtosecond timescale[115–119]. Even pump–probe techniques are too slow. Instead, the chirp of the attosecond pulse (attochirp) is used to give temporal resolution that is shorter than the pulse itself; different photon energies are produced by electrons recolliding at slightly different times (BOX 3). An experiment was designed to observe charge migration in iodoacetylene molecules[120,121], as seen in FIG. 5. First, the gas-phase molecules were oriented in space, meaning that not only was the molecular axis aligned but also the head-to-tail direction was oriented[70]. Second, an intense laser pulse was used to drive HHG in the molecules, and the HHG spectrum was recorded. Because the polar molecules were oriented in space, the left–right symmetry of the electron trajectories in HHG was broken, leading to the emission of even harmonics of the driving laser frequency. The ratio of even to odd harmonics gave insight into the phase difference of each emitted harmonic order. However, the important information came from the subcycle timescale. The iodoacetylene molecule could be ionized near the peak of each optical cycle, this effectively being the start trigger for the measurement. As in the CO_2 experiments[79], two electronic states of the cation were produced by the strong-field ionization, that is, the X (ground state, 9.71 eV) and A (first excited state, 11.94 eV) states. Because the states were prepared coherently, an electronic wavepacket was produced. Because an electron was removed, this was a hole wavepacket. Depending on the time at which the electron recombined with the molecular ion, the hole wavepacket was in a different location along the molecular axis. To put it another way, the phase between the two states evolved in time. Two laser wavelengths were used, that is, 800 nm and 1,300 nm, to disentangle the timing. A sophisticated model was used to deduce that the hole wavepacket started at the iodine end of the molecule, travelled to the other end, then returned to the iodine, within a period of 1.8 fs. When the molecular axis was perpendicular to the laser polarization, the hole wavepacket moved independently of the field, but when it was parallel, the wavepacket was strongly influenced by the laser field.

Conclusions

The use of attosecond techniques to study fixed-in-space molecules has opened up new opportunities to study the electronic structure of molecules. The field of high harmonic spectroscopy has grown out of these techniques and has permitted the imaging of molecular orbitals. In parallel, using high harmonics as a photoionizing source permits the measurement of transition dipole matrix elements in the molecular frame and the complete characterization of the partial wave composition of photoionization channels[122]. In a pump–probe configuration, high harmonic spectroscopy can follow unimolecular chemical reactions with a time resolution of 10 fs. Sub-femtosecond measurement of charge migration within molecules is possible owing to the subcycle dynamics of the high harmonic process. Other attosecond techniques, such as attosecond transient absorption spectroscopy, can be used to probe the electronic structure of atoms and molecules[123–136].

By using higher photon energies, particularly those near the carbon K-edge around 284 eV, it is possible to remove a core 1s electron with low kinetic energy; the absorption spectrum near the K-edge shows features that are related to the molecular structure in a process such as near-edge X-ray absorption fine structure[137–139].

1. McPherson, A. et al. Studies of multiphoton production of vacuum-ultraviolet radiation in the rare gases. *JOSA B* **4**, 595 (1987).
2. Li, J. et al. 53-attosecond X-ray pulses reach the carbon K-edge. *Nat. Commun.* **8**, 186 (2017).
3. Gaumnitz, T. et al. Streaking of 43-attosecond soft-X-ray pulses generated by a passively CEP-stable mid-infrared driver. *Opt. Express* **25**, 27506–27518 (2017).
4. Scrinzi, A., Ivanov, M. Y., Kienberger, R. & Villeneuve, D. M. Attosecond physics. *J. Phys. B. At. Mol. Opt. Phys.* **39**, R1–R37 (2006).
5. Corkum, P. B. & Krausz, F. Attosecond science. *Nat. Phys.* **3**, 381–387 (2007).
6. Krausz, F. & Ivanov, M. Attosecond physics. *Rev. Mod. Phys.* **81**, 163–234 (2009).
7. Haessler, S., Caillat, J. & Salières, P. Self-probing of molecules with high harmonic generation. *J. Phys. B. At. Mol. Opt. Phys.* **44**, 203001 (2011).
8. Gallmann, L., Cirelli, C. & Keller, U. Attosecond science: recent highlights and future trends. *Annu. Rev. Phys. Chem.* **63**, 447–469 (2012).
9. Leone, S. R. et al. What will it take to observe processes in 'real time'? *Nat. Photonics* **8**, 162 (2014).
10. Azoury, D. et al. Self-probing spectroscopy of XUV photo-ionization dynamics in atoms subjected to a strong-field environment. *Nat. Commun.* **8**, 1453 (2017).
11. Uiberacker, M. et al. Attosecond real-time observation of electron tunnelling in atoms. *Nature* **446**, 627–632 (2007).
12. Goulielmakis, E. et al. Real-time observation of valence electron motion. *Nature* **466**, 739–743 (2010).
13. Eckle, P. et al. Attosecond ionization and tunneling delay time measurements in helium. *Science* **322**, 1525–1529 (2008).
14. Sansone, G. et al. Electron localization following attosecond molecular photoionization. *Nature* **465**, 763–766 (2010).
15. Takahashi, E. J., Lan, P., Mücke, O. D., Nabekawa, Y. & Midorikawa, K. Attosecond nonlinear optics using gigawatt-scale isolated attosecond pulses. *Nat. Commun.* **4**, 2691 (2013).
16. Villeneuve, D. M., Hockett, P., Vrakking, M. J. J. & Niikura, H. Coherent imaging of an attosecond electron wave packet. *Science* **356**, 1150–1153 (2017).
17. Kling, M. F. & Vrakking, M. J. J. Attosecond electron dynamics. *Annu. Rev. Phys. Chem.* **59**, 463–492 (2008).
18. Gruson, V. et al. Attosecond dynamics through a Fano resonance: monitoring the birth of a photoelectron. *Science* **354**, 734–738 (2016).
19. Trabattoni, A. et al. Mapping the dissociative ionization dynamics of molecular nitrogen with attosecond time resolution. *Phys. Rev. X* **5**, 041053 (2015).
20. Schultze, M. et al. Delay in photoemission. *Science* **328**, 1658–1662 (2010).
21. Klünder, K. et al. Probing single-photon ionization on the attosecond time scale. *Phys. Rev. Lett.* **106**, 143002 (2011).
22. Kobayashi, Y. et al. Selectivity of electronic coherence and attosecond ionization delays in strong-field double ionization. *Phys. Rev. Lett.* **120**, 233201 (2018).
23. Sabbar, M. et al. Resonance effects in photoemission time delays. *Phys. Rev. Lett.* **115**, 133001 (2015).
24. Hockett, P., Frumker, E., Villeneuve, D. M. & Corkum, P. B. Time delay in molecular photoionization. *J. Phys. B. At. Mol. Opt. Phys.* **49**, 095602 (2016).
25. Huppert, M., Jordan, I., Baykusheva, D., von Conta, A. & Wörner, H. J. Attosecond delays in molecular photoionization. *Phys. Rev. Lett.* **117**, 093001 (2016).
26. Vos, J. et al. Orientation-dependent stereo Wigner time delay and electron localization in a small molecule. *Science* **360**, 1326–1330 (2018).
27. Baykusheva, D. & Wörner, H. J. Theory of attosecond delays in molecular photoionization. *J. Chem. Phys.* **146**, 124306 (2017).
28. Schoun, S. B. et al. Precise access to the molecular-frame complex recombination dipole through high-harmonic spectroscopy. *Phys. Rev. Lett.* **118**, 033201 (2017).
29. Gallmann, L. et al. Photoemission and photoionization time delays and rates. *Struct. Dyn.* **4**, 061502 (2017).
30. Kotur, M. et al. Spectral phase measurement of a Fano resonance using tunable attosecond pulses. *Nat. Commun.* **7**, 10566 (2016).
31. Isinger, M. et al. Photoionization in the time and frequency domain. *Science* **362**, eaao7043 (2017).
32. Itatani, J. et al. Tomographic imaging of molecular orbitals. *Nature* **432**, 867–871 (2004).
33. Le, A.-T., Lucchese, R. R. & Lin, C. D. Quantitative rescattering theory of high-order harmonic generation for polyatomic molecules. *Phys. Rev. A.* **87**, 063406 (2013).
34. Frolov, M. V. et al. Analytic description of the high-energy plateau in harmonic generation by atoms: can the harmonic power increase with increasing laser wavelengths? *Phys. Rev. Lett.* **102**, 243901–4 (2009).
35. Frolov, M. V., Manakov, N. L., Sarantseva, T. S. & Starace, A. F. Analytic formulae for high harmonic generation. *J. Phys. B* **42**, 035601 (2009).
36. Drescher, M. et al. X-ray pulses approaching the attosecond frontier. *Science* **291**, 1923–1927 (2001).
37. Hentschel, M. et al. Attosecond metrology. *Nature* **414**, 509–513 (2001).
38. Popmintchev, T. et al. Bright coherent ultrahigh harmonics in the keV X-ray regime from mid-infrared femtosecond lasers. *Science* **336**, 1287–1291 (2012).
39. Corkum, P. B. Plasma perspective on strong field multiphoton ionization. *Phys. Rev. Lett.* **71**, 1994 (1993).
40. Balcou, P., Salières, P., L'Huillier, A. & Lewenstein, M. Generalized phase-matching conditions for high harmonics: the role of field-gradient forces. *Phys. Rev. A.* **55**, 3204–3210 (1997).
41. Christov, I. P., Murnane, M. M. & Kapteyn, H. C. High-harmonic generation of attosecond pulses in the "single-cycle" regime. *Phys. Rev. Lett.* **78**, 1251–1254 (1997).
42. Sansone, G. et al. Isolated single-cycle attosecond pulses. *Science* **314**, 443 (2006).
43. Goulielmakis, E. et al. Single-cycle nonlinear optics. *Science* **320**, 1614–1617 (2008).
44. Ferrari, F. et al. High-energy isolated attosecond pulses generated by above-saturation few-cycle fields. *Nat. Photonics* **4**, 875–879 (2010).
45. Mashiko, H. et al. Double optical gating of high-order harmonic generation with carrier-envelope phase stabilized lasers. *Phys. Rev. Lett.* **100**, 103906 (2008).
46. Baltuška, A. et al. Attosecond control of electronic processes by intense light fields. *Nature* **421**, 611–615 (2003).
47. Zhao, K. et al. Tailoring a 67 attosecond pulse through advantageous phase-mismatch. *Opt. Lett.* **37**, 3891–3893 (2012).
48. Cooper, J. W. Photoionization from outer atomic subshells. A model study. *Phys. Rev.* **128**, 681 (1962).
49. Samson, J. A. R. & Stolte, W. C. Precision measurements of the total photoionization cross-sections of He, Ne, Ar, Kr, and Xe. *J. Electron Spectrosc. Relat. Phenom.* **123**, 265 (2002).
50. Wörner, H. J., Niikura, H., Bertrand, J. B., Corkum, P. B. & Villeneuve, D. M. Observation of electronic structure minima in high-harmonic generation. *Phys. Rev. Lett.* **102**, 103901 (2009).
51. Higuet, J. et al. High-order harmonic spectroscopy of the Cooper minimum in argon: experimental and theoretical study. *Phys. Rev. A.* **83**, 053401 (2011).
52. Zhou, J., Peatross, J., Murnane, M. M., Kapteyn, H. C. & Christov, I. P. Enhanced high-harmonic generation using 25 fs laser pulses. *Phys. Rev. Lett.* **76**, 752–755 (1996).
53. Minemoto, S. et al. Retrieving photorecombination cross sections of atoms from high-order harmonic spectra. *Phys. Rev. A.* **78**, 061402 (2008).
54. Wong, M. C. H. et al. High harmonic spectroscopy of the Cooper minimum in molecules. *Phys. Rev. Lett.* **110**, 033006 (2013).
55. Wahlström, C.-G. et al. High-order harmonic generation in rare gases with an intense short-pulse laser. *Phys. Rev. A.* **48**, 4709–4720 (1993).
56. Farrell, J. P. et al. Influence of phase matching on the Cooper minimum in Ar high-order harmonic spectra. *Phys. Rev. A.* **83**, 023420 (2011).
57. Becker, U. et al. Subshell photoionization of Xe between 40 and 1000 eV. *Phys. Rev. A.* **39**, 3902–3911 (1989).
58. Amusia, M. Y. & Connerade, J.-P. The theory of collective motion probed by light. *Rep. Prog. Phys.* **63**, 41 (2000).
59. Shiner, A. D. et al. Probing collective multi-electron dynamics in xenon with high-harmonic spectroscopy. *Nat. Phys.* **7**, 464–467 (2011).
60. Pabst, S. & Santra, R. Strong-field many-body physics and the giant enhancement in the high-harmonic spectrum of xenon. *Phys. Rev. Lett.* **111**, 233005 (2013).
61. Mairesse, Y., Levesque, J., Dudovich, N., Corkum, P. B. & Villeneuve, D. M. High harmonic generation from aligned molecules — amplitude and polarization. *J. Mod. Opt.* **55**, 2591–2602 (2008).
62. Kanai, T., Minemoto, S. & Sakai, H. Quantum interference during high-order harmonic generation from aligned molecules. *Nat. Lond.* **435**, 470–474 (2005).
63. Stapelfeldt, H. & Seideman, T. Aligning molecules witht strong laser pulses. *Rev. Mod. Phys.* **75**, 543–557 (2003).
64. Rosca-Pruna, F. & Vrakking, M. J. J. Experimental onservation of revival structure in picosecond laer-induced alignment of I_2. *Phys. Rev. Lett.* **87**, 153902 (2001).
65. Yun, H., Yun, S. J., Lee, G. H. & Nam, C. H. High-harmonic spectroscopy of aligned molecules. *J. Phys. B. At. Mol. Opt. Phys.* **50**, 022001 (2017).
66. Ramakrishna, S. & Seideman, T. Information content of high harmonics generated from aligned molecules. *Phys. Rev. Lett.* **99**, 113901 (2007).
67. Torres, R. et al. Probing orbital structure of polyatomic molecules by high-order harmonic Generation. *Phys. Rev. Lett.* **98**, 203007 (2007).
68. Zhou, X. X., Tong, X. M., Zhao, Z. X. & Lin, C. D. Role of molecular orbital symmetry on the alignment dependence of high-order harmonic generation with molecules. *Phys. Rev. A.* **71**, 061801 (2005).
69. De, S. et al. Field-free orientation of CO molecules by femtosecond two-color laser fields. *Phys. Rev. Lett.* **103**, 153002 (2009).
70. Kraus, P. M., Baykusheva, D. & Wörner, H. J. Two-pulse field-free orientation reveals anisotropy of molecular shape Resonance. *Phys. Rev. Lett.* **113**, 023001 (2014).
71. Kraus, P. M. et al. Observation of laser-induced electronic structure in oriented polyatomic molecules. *Nat. Commun.* **6**, 7039 (2015).
72. Frumker, E. et al. Oriented rotational wave-packet dynamics studies via high harmonic generation. *Phys. Rev. Lett.* **109**, 113901 (2012).
73. Frumker, E. et al. Probing polar molecules with high harmonic spectroscopy. *Phys. Rev. Lett.* **109**, 233904 (2012).
74. Kraus, P. M., Rupenyan, A. & Wörner, H. J. High-harmonic spectroscopy of oriented OCS molecules: emission of even and odd harmonics. *Phys. Rev. Lett.* **109**, 233903 (2012).
75. Lein, M., Hay, N., Velotta, R., Marangos, J. P. & Knight, P. L. Role of the intramolecular phase in high-harmonic generation. *Phys. Rev. Lett.* **88**, 183903 (2002).
76. Hay, N. et al. High-order harmonic generation in laser-aligned molecules. *Phys. Rev. A.* **65**, 053805 (2002).
77. Vozzi, C. et al. Controlling two-center interference in molecular high harmonic generation. *Phys. Rev. Lett.* **95**, 153902 (2005).
78. Torres, R. et al. Revealing molecular structure and dynamics through high-order harmonic generation driven by mid-IR fields. *Phys. Rev. A.* **81**, 051802 (2010).
79. Smirnova, O. et al. High harmonic interferometry of multi-electron dynamics in molecules. *Nature* **460**, 972–977 (2009).
80. Worner, H. J., Bertrand, J. B., Hockett, P., Corkum, P. B. & Villeneuve, D. M. Controlling the interference of multiple molecular orbitals in high-harmonic generation. *Phys. Rev. Lett.* **104**, 233904 (2010).
81. Jin, C., Le, A.-T. & Lin, C. D. Analysis of effects of macroscopic propagation and multiple molecular orbitals on the minimum in high-order harmonic generation of aligned CO_2. *Phys. Rev. A.* **83**, 053409 (2011).
82. McFarland, B. K., Farrell, J. P., Bucksbaum, P. H. & Gühr, M. High harmonic generation from multiple orbitals in N_2. *Science* **322**, 1232–1235 (2008).
83. Le, A.-T., Lucchese, R. R. & Lin, C. D. Uncovering multiple orbitals influence in high harmonic generation from aligned N_2. *J. Phys. B. At. Mol. Opt. Phys.* **42**, 211001 (2009).
84. Lee, G. H. et al. Alignment dependence of high harmonics contributed from HOMO and HOMO-1 orbitals of N_2 molecules. *J. Phys. B. At. Mol. Opt. Phys.* **43**, 205602 (2010).
85. Paul, P. M. et al. Observation of a train of attosecond pulses from high harmonic generation. *Science* **292**, 1689–1692 (2001).
86. Mairesse, Y. et al. Attosecond synchronization of high-harmonic soft X-rays. *Science* **302**, 1540–1543 (2003).

87. Zhou, X. et al. Molecular recollision interferometry in high harmonic generation. *Phys. Rev. Lett.* **100**, 073902 (2008).
88. Bertrand, J. B., Wörner, H. J., Salières, P., Villeneuve, D. M. & Corkum, P. B. Linked attosecond phase interferometry for molecular frame measurements. *Nat. Phys.* **9**, 174–178 (2013).
89. Wagner, N. L. et al. Monitoring molecular dynamics using coherent electrons from high harmonic generation. *Proc. Natl. Acad. Sci. U.S.A.* **103**, 13279–13285 (2006).
90. McFarland, B. K., Farrell, J. P., Bucksbaum, P. H. & Guhr, M. High-order harmonic phase in molecular nitrogen. *Phys. Rev. A.* **80**, 033412 (2009).
91. Shafir, D. et al. Resolving the time when an electron exits a tunnelling barrier. *Nature* **485**, 343 (2012).
92. Niikura, H., Dudovich, N., Villeneuve, D. M. & Corkum, P. B. Mapping molecular orbital symmetry on high-order harmonic generation spectrum using two-color laser fields. *Phys. Rev. Lett.* **105**, 053003 (2010).
93. Niikura, H., Wörner, H. J., Villeneuve, D. M. & Corkum, P. B. Probing the spatial structure of a molecular attosecond electron wave packet using shaped recollision trajectories. *Phys. Rev. Lett.* **107**, 093004 (2011).
94. Kim, I. J. et al. Highly efficient high-harmonic generation in an orthogonally polarized two-color laser field. *Phys. Rev. Lett.* **94**, 243901 (2005).
95. Raz, O., Pedatzur, O., Bruner, B. D. & Dudovich, N. Spectral caustics in attosecond science. *Nat. Photonics* **6**, 170–173 (2012).
96. Yun, H. et al. Resolving multiple molecular orbitals using two-dimensional high-harmonic spectroscopy. *Phys. Rev. Lett.* **114**, 153901 (2015).
97. Zhou, X. et al. Elliptically polarized high-order harmonic emission from molecules in linearly polarized laser fields. *Phys. Rev. Lett.* **102**, 073902–4 (2009).
98. Mairesse, Y. et al. High harmonic spectroscopy of multichannel dynamics in strong-field ionization. *Phys. Rev. Lett.* **104**, 213601 (2010).
99. Fleischer, A., Kfir, O., Diskin, T., Sidorenko, P. & Cohen, O. Spin angular momentum and tunable polarization in high-harmonic generation. *Nat. Photonics* **8**, 543–549 (2014).
100. Kfir, O. et al. Generation of bright phase-matched circularly-polarized extreme ultraviolet high harmonics. *Nat. Photonics* **9**, 99–105 (2015).
101. Fan, T. et al. Bright circularly polarized soft X-ray high harmonics for X-ray magnetic circular dichroism. *Proc. Natl. Acad. Sci. U.S.A.* **112**, 14206–14211 (2015).
102. Gariepy, G. et al. Creating high-harmonic beams with controlled orbital angular momentum. *Phys. Rev. Lett.* **113**, 153901 (2014).
103. Kong, F. et al. Controlling the orbital angular momentum of high harmonic vortices. *Nat. Commun.* **8**, 14970 (2017).
104. Zhai, C. et al. Diffractive molecular-orbital tomography. *Phys. Rev. A.* **95**, 033420 (2017).
105. Haessler, S. et al. Attosecond imaging of molecular electronic wavepackets. *Nat. Phys.* **6**, 200–206 (2010).
106. Boutu, W. et al. Coherent control of attosecond emission from aligned molecules. *Nat. Phys.* **4**, 545–549 (2008).
107. Vozzi, C. et al. Generalized molecular orbital tomography. *Nat. Phys.* **7**, 822–826 (2011).
108. Li, W. et al. Time-resolved dynamics in N_2O_4 probed using high harmonic generation. *Science* **322**, 1207–1211 (2008).
109. Baker, S. et al. Probing proton dynamics in molecules on an attosecond time scale. *Science* **312**, 424 (2006).
110. Lan, P. et al. Attosecond probing of nuclear dynamics with trajectory-resolved high-harmonic spectroscopy. *Phys. Rev. Lett.* **119**, 033201 (2017).
111. Wörner, H. J. et al. Conical intersection dynamics in NO_2 probed by homodyne high-harmonic spectroscopy. *Science* **334**, 208–212 (2011).
112. Worner, H. J., Bertrand, J. B., Kartashov, D. V., Corkum, P. B. & Villeneuve, D. M. Following a chemical reaction using high-harmonic interferometry. *Nature* **466**, 604–607 (2010).
113. Ruf, H. et al. High-harmonic transient grating spectroscopy of NO_2 electronic relaxation. *J. Chem. Phys.* **137**, 224303 (2012).
114. Kraus, P. M. et al. High-harmonic probing of electronic coherence in dynamically aligned molecules. *Phys. Rev. Lett.* **111**, 243005 (2013).
115. Wörner, H. J. et al. Charge migration and charge transfer in molecular systems. *Struct. Dyn.* **4**, 061508 (2017).
116. Calegari, F. et al. Charge migration induced by attosecond pulses in bio-relevant molecules. *J. Phys. B. At. Mol. Opt. Phys.* **49**, 142001 (2016).
117. Lépine, F., Ivanov, M. Y. & Vrakking, M. J. J. Attosecond molecular dynamics: fact or fiction? *Nat. Photonics* **8**, 195 (2014).
118. Belshaw, L. et al. Observation of ultrafast charge migration in an amino acid. *J. Phys. Chem. Lett.* **3**, 3751–3754 (2012).
119. Calegari, F. et al. Ultrafast electron dynamics in phenylalanine initiated by attosecond pulses. *Science* **346**, 336 (2014).
120. Kraus, P. M. et al. Measurement and laser control of attosecond charge migration in ionized iodoacetylene. *Science* **350**, 790–795 (2015).
121. Kraus, P. M. & Wörner, H. J. Perspectives of attosecond spectroscopy for the understanding of fundamental electron correlations. *Angew. Chem. Int. Ed.* **57**, 5228–5247 (2018).
122. Marceau, C. et al. Molecular frame reconstruction using time-domain photoionization interferometry. *Phys. Rev. Lett.* **119**, 083401 (2017).
123. Beck, A. R., Neumark, D. M. & Leone, S. R. Probing ultrafast dynamics with attosecond transient absorption. *Chem. Phys. Lett.* **624**, 119–130 (2015).
124. Chatterley, A. S., Lackner, F., Neumark, D. M., Leone, S. R. & Gessner, O. Tracking dissociation dynamics of strong-field ionized 1,2-dibromoethane with femtosecond XUV transient absorption spectroscopy. *Phys. Chem. Chem. Phys.* **18**, 14644–14653 (2016).
125. Warrick, E. R., Cao, W., Neumark, D. M. & Leone, S. R. Probing the dynamics of Rydberg and valence states of molecular nitrogen with attosecond transient absorption spectroscopy. *J. Phys. Chem. A* **120**, 3165–3174 (2016).
126. Attar, A. R., Bhattacherjee, A. & Leone, S. R. Direct observation of the transition-state region in the photodissociation of CH_3I by femtosecond extreme ultraviolet transient absorption spectroscopy. *J. Phys. Chem. Lett.* **6**, 5072–5077 (2015).
127. Cheng, Y. et al. Reconstruction of an excited-state molecular wave packet with attosecond transient absorption spectroscopy. *Phys. Rev. A.* **94**, 023403 (2016).
128. Reduzzi, M. et al. Observation of autoionization dynamics and sub-cycle quantum beating in electronic molecular wave packets. *J. Phys. B. At. Mol. Opt. Phys.* **49**, 065102 (2016).
129. Cao, W., Warrick, E. R., Fidler, A., Leone, S. R. & Neumark, D. M. Excited-state vibronic wave-packet dynamics in H_2 probed by XUV transient four-wave mixing. *Phys. Rev. A.* **97**, 023401 (2018).
130. Warrick, E. R. et al. Attosecond transient absorption spectroscopy of molecular nitrogen: vibrational coherences in the $b'\ ^1\Sigma^+_u$ state. *Chem. Phys. Lett.* **683**, 408–415 (2017).
131. Liao, C.-T. et al. Probing autoionizing states of molecular oxygen with XUV transient absorption: electronic-symmetry-dependent line shapes and laser-induced modifications. *Phys. Rev. A.* **95**, 043427 (2017).
132. Ott, C. et al. Lorentz meets Fano in spectral line shapes: a universal phase and its laser control. *Science* **340**, 716–720 (2013).
133. Kaldun, A. et al. Observing the ultrafast buildup of a Fano resonance in the time domain. *Science* **354**, 738–741 (2016).
134. Ott, C. et al. Reconstruction and control of a time-dependent two-electron wave packet. *Nature* **516**, 374–378 (2014).
135. Sabbar, M. et al. State-resolved attosecond reversible and irreversible dynamics in strong optical fields. *Nat. Phys.* **13**, 472–478 (2017).
136. Chini, M. et al. Subcycle ac stark shift of helium excited states probed with isolated attosecond pulses. *Phys. Rev. Lett.* **109**, 073601 (2012).
137. Teichmann, S. M., Silva, F., Cousin, S. L., Hemmer, M. & Biegert, J. 0.5-keV Soft X-ray attosecond continua. *Nat. Commun.* **7**, 11493 (2016).
138. Attar, A. R. et al. Femtosecond X-ray spectroscopy of an electrocyclic ring-opening reaction. *Science* **356**, 54–59 (2017).
139. Popmintchev, D. et al. Near- and extended-edge X-ray-absorption fine-structure spectroscopy using ultrafast coherent high-order harmonic supercontinua. *Phys. Rev. Lett.* **120**, 093002 (2018).

Author contributions
The authors contributed equally to all aspects of the article.

Competing interests
The authors declare no competing interests.

Supplementary information
Supplementary information is available for this paper at https://doi.org/10.1038/s42254-018-0015-1.